Phosphorylated lignin–cellulose nanofibrils for multifunctional PVA composites with UV-absorption and flame-retardancy

Soumia Boukind, Wafa Cheikhrouhou, Jean-Luc Putaux, Sami Boufi, Houssine Sehaqui

Phosphorylated lignin–cellulose nanofibrils for multifunctional PVA composites with UV-absorption and flame-retardancy

Soumia Boukind[a,*], Wafa Cheikhrouhou[b], Jean-Luc Putaux[c]
Sami Boufi[b,*], Houssine Sehaqui[a,*]

[a] *Materials Science, Energy and Nanoengineering (MSN) Department, Mohammed VI Polytechnic University, Lot660 – Hay Moulay Rachid, 43150 Benguerir, Morocco*
[b] *LMSE, Faculty of Science, University of Sfax, Sfax BP 802–3018, Tunisia*
c *Univ. Grenoble Alpes, CNRS, CERMAV, F-38000 Grenoble, France*

Published in: **Composites Part A**, *201* (2026), 109421
DOI: 10.1016/j.compositesa.2025.109421

Abstract

Composite manufacturing often requires multiple additives to achieve desired properties in terms of strength, safety, and durability. Here, we produce multifunctional lignin-cellulose nanofibrils (PLCNFs) via a simple phosphorylation of giant reed using H_3PO_4/urea. The synergistic effects of cellulose, lignin, and phosphate in PLCNFs offer promising prospects for the manufacturing of multifunctional composites. Polyvinyl alcohol (PVA)/PLCNF nanocomposites were produced by solvent casting and comprehensively characterized using scanning electron microscopy, thermogravimetric analysis, differential scanning calorimetry, Fourier transform infrared (FTIR) spectroscopy, UV–vis spectroscopy, contact angle measurements, moisture uptake, and microscale combustion calorimetry. The reinforcing and flame-retardant potentials of PLCNF in the PVA matrix were revealed, along with additional UV-shielding and hydrophobicity imparted by lignin. These features highlight the potential applications of these nanocomposites as a safe substitute for flammable or hazardous materials. These multifunctional films are promising for sustainable food packaging and protective coating applications requiring UV-blocking and flame-retardant properties. In summary, this study demonstrates that underused lignocellulosic resources, when combined with benign phosphorylation chemistry, can serve as robust, reliable, and eco-friendly flame-retardant additives for enhanced nanocomposites.

1. Introduction

The development of polymeric materials with enhanced properties often relies on the incorporation of reinforcing fibers and particulate additives to improve specific properties such as strength, stiffness, thermal stability, and flame retardancy [1,2]. Such composites have garnered significant interest for applications requiring both durability and lightweight properties, including the aerospace, automotive, construction, and sports equipment sectors, where the polymer matrix alone is insufficient. Natural fiber composites use fibers derived from renewable biological sources to provide mechanical reinforcement, offering a sustainable alternative to synthetic fibers (e.g., glass and carbon fibers) with reduced environmental impact, lower cost, and enhanced biodegradability. Nonetheless, these composites exhibit inherent limitations, such as high moisture uptake, poor interfacial adhesion with hydrophobic polymer matrices, and susceptibility to thermal degradation [3]. These challenges can be addressed by incorporating functional additives, such as stabilizers against thermal and oxidative degradation, UV absorbers, and flame-retardant nanofillers [4].

In recent years, cellulose nanomaterials, particularly cellulose nanocrystals (CNCs) and cellulose nanofibrils (CNFs), have attracted substantial attention in the field of bio-based composites due to their exceptional mechanical properties, renewability, biodegradability, and ability to form strong percolating networks within polymer matrices [5]. Cellulose nanomaterials have been used as rheology modifiers in coatings and adhesives, as well as reinforcing agents in polymer matrices, additionally enhancing their barrier properties [6]. These nanomaterials are typically produced from cellulosic pulp using chemical, enzymatic, and/or mechanical treatments, yielding high surface area nanofibrils or nanorods suspended in water, which facilitates their integration into water-based polymer matrices for composite production [7]. The pulp is commonly derived from wood, plants, algae, or agricultural residues through chemical processes that aim to isolate cellulose from other biopolymeric components [8]. Yet, conventional pulping methods often remove lignin, a multifunctional biopolymer integral to the plant cell wall that provides added value when associated with cellulose nanomaterials. Its complex chemical structure imparts rigidity, hydrophobicity, and protective functions, thereby enhancing durability under environmental conditions [9]. Therefore, incorporating lignin into composite design, inspired by plant architecture, enables the development of multifunctional materials with improved mechanical, thermal, UV, and moisture resistance, complementing the inherent strength and barrier performance of cellulose nanomaterials [10].

Recent research has focused on engineering lignin-cellulose nanofibrils (LCNFs), which combine the mechanical strength of cellulose with the functional versatility of lignin. The

incorporation of lignin micro- and nanostructures enhances hydrophobicity, thermal stability, UV resistance, and compatibility with non-polar polymer matrices. To facilitate the mechanical disintegration of lignocellulosic biomass into nanomaterial elements, enzymatic or chemical pretreatments are commonly employed to reduce energy consumption during the fibrillation process. Pretreatment methods such as TEMPO-oxidation, phosphorylation, and hydrothermal processing with organic acids have been investigated [9,11]. Phosphorylation has been reported as a green approach for producing CNFs with grafted phosphate moieties that promote fibril dispersion through electrostatic repulsion and impart inherent flame-retardant properties [12]. Emerging research has further revealed the benefits of phosphorylated lignocellulosic nanofibrils (PLCNFs) for functional materials. Xu et al. developed a multifunctional PLCNFs hydrogel with mechanical robustness, conductivity, and self-healing, for electronic devices in healthcare monitoring [13]. Similarly, a recent work reported the rapid fabrication of PLCNF-based amphibious hydrogels with outstanding motion-sensing ability, high conductivity, and good water resistance for advanced flexible electronics [14]. These findings support the strong potential of PLCNFs beyond hydrogels, particularly in polymer composite applications where simultaneous mechanical reinforcement and flame retardancy are highly required.

The advancement of multifunctional lignocellulosic nanomaterials via scalable, cost-effective, and environmentally benign phosphorylation techniques is expected to drive industrial interest in developing multifunctional composites and to address the limitations of lignin-free CNF. Several studies have investigated LCNFs as reinforcing fillers in different polymer matrices, including polylactic acid (PLA), Polyvinyl alcohol (PVA), and polypropylene (PP) [15], [16], [17]. Poly(vinyl alcohol) (PVA) is a biodegradable synthetic polymer recognized for its superior performance in various applications [18]. Zhang et al. investigated the incorporation of oxidized LCNFs (t-LCNF) as nanofillers in a PVA matrix, which promoted homogenous dispersion and formation of strong intermolecular H-bonding. At loadings of t-LCNF up to 10 wt%, the resulting PVA films demonstrated enhanced tensile strength, Young's modulus, and toughness, along with improved thermal stability, hydrophobicity, and effective UV-shielding ability [19]. In a previous study, LCNFs derived from unbleached pulps was incorporated as a reinforcing agent in a PVA matrix, resulting in a significant improvement in mechanical and thermal performance, particularly with high lignin content PLCNFs (~22.1 wt%) [20]. Another study by Zhang et al. reported a low-cost and environmentally friendly strategy to broaden PVA applications by incorporating LCNFs as a multifunctional component in high-performance composites [10]. The inclusion of LCNFs into the PVA matrix enhanced its mechanical and thermal properties, while providing additional attributes such as high hydrophobicity and low water vapor transmission. However, LCNFs

bearing flame-retardant phosphate moieties have yet to be explored as composite reinforcements, despite their exceptional potential to simultaneously enhance strength, safety, and durability through a single phosphorylated LCNF (PLCNFs) component. Moreover, PLCNFs-based composites could offer improved end-of-life disposal options due to their bio-based origin and potential biodegradability.

To the best of our knowledge, the present study is the first to demonstrate eco-friendly and straightforward phosphorylation of unbleached Giant reed (*Arundo donax*) using a phosphoric acid/urea system to produce multifunctional phosphorylated lignin-cellulose nanofibrils (PLCNFs) destined for enhancing the strength, safety, and durability of polymer-based composites, offering a sustainable approach with strong potential for scale-up. This strategy uniquely retains lignin while simultaneously incorporating phosphate moieties into the fibril structure, providing a single multifunctional nanomaterial that combines mechanical reinforcement, UV-shielding, and flame-retardant performance. In this work, PLCNFs derived from the fast-growing and highly renewable perennial grass are incorporated into PVA to produce high-performance composite films, providing an alternative to conventional wood-based feedstocks that rely on slower-growing resources and more resource-intensive processes. The mechanical, thermal, UV-absorption, flame-retardant, and hygroscopic properties of these composites are investigated and compared with those of state-of-the-art PVA composites reinforced with natural nanofibers, with particular emphasis on elucidating the functional role of lignin. Achieving this combination of functionalities directly from unbleached lignocellulosic biomass and applying PLCNFs to composite films represents a novel contribution that has not been reported previously in CNF-based systems. The simplicity of the processing enables scalable fabrication of high-performance materials for advanced packaging applications.

2. Experimental

2.1. Materials

Raw Giant reed fibers (LCFs; *Arundo donax* L.*)* were collected from the region of Benguerir, Rehamna province, in central Morocco. The chemical composition of the fibers is approximately 60.4 wt% cellulose, 23.4 wt% lignin, and 19.2 wt% hemicellulose [21]. Orthophosphoric acid (H_3PO_4, 85 wt%), urea (CH_4N_2O), PVA (Mw=130,000, 99+% hydrolyzed), and sodium hydroxide (NaOH, >97 %) were purchased from Scharlab, Solvachim, and Sigma-Aldrich, respectively. All chemical reagents were of analytical grade and used as received without further purification.

2.2. PLCNF production

Ground giant reed fibers were impregnated with a solution containing urea and phosphoric acid at a mass ratio of 1:2:2 (fibers:urea:PA) at a solid to liquid ratio of 1:10. The mixture was allowed to rest for 30 min at room temperature, followed by drying overnight in a ventilated oven at 60 °C. Next, the dried fibers were cured at 140 °C for 1 h and subsequently washed thoroughly with distilled water. The resulting phosphorylated fibers were alkali-treated with a 1 M NaOH solution (solid to liquid ratio of 1:10), repeatedly washed with distilled water, and blended at a concentration of 2 wt%. The suspension was then passed once through a microfluidizer (M110Y, Microfluidics Corp., USA) equipped with sequential disintegration chambers of 200 and 100 µm, operating at a pressure of 1500 bar. The obtained PLCNF suspension (2 wt%) was stored at 4 °C for further characterization. Supplementary Information Fig. SI1 illustrates a schematic overview of the PLCNF production process.

2.3. Preparation of PVA/PLCNF nanocomposite films

Solvent casting technique was performed to prepare neat PVA, neat PLCNF, and PVA/PLCNF reinforced nanocomposite films at different PLCNF contents (5, 10, 15, and 20 wt%) **(**Fig. SI2**)**. A solution of 5 wt% PVA was prepared by dissolving 12 g of PVA in 240 mL of distilled water at 90 °C for 1 h with continuous stirring. After cooling the solution at room temperature, the composite formulations were prepared by blending the PVA solution with a specific amount of PLCNFs at room temperature under magnetic stirring. The resulting PVA/PLCNF formulations were ultimately cast onto circular Petri dishes and air-dried for several days at room temperature. Neat PVA and PLCNF films were prepared using the same procedure stated above. The produced films were designated as PVA, PLCNF, PLCNF-5, PLCNF-10, PLCNF-15, and PLCNF-20, where the number represents the weight loading of PLCNF in each film.

2.4. Characterization

PLCNF suspensions were observed by transmission electron microscopy using a JEOL JEM 2100-Plus microscope operating at 200 kV. Droplets of dilute nanocellulose suspensions were deposited onto glow-discharged carbon-coated copper grids and stained with 2 wt% uranyl acetate. Images were then recorded on a Gatan Rio 16 camera.

Cross-sections of the cryofractured nanocomposite films were analyzed by scanning electron microscopy (EVO 10, Zeiss) operated at an acceleration voltage of 15 kV. Samples were mounted on carbon tape and sputter-coated with gold under vacuum. Cross-sectional surfaces were prepared by fracturing the films in liquid nitrogen before coating.

The charge content of PLCNF was determined by potentiometric titration after converting the PLCNF into their protonated form using a strong-acid cation-exchange resin (H^+ form: Amberlyst® 15H^+). Briefly, 0.10 g of dried PLCNFs was dispersed in 25 mL of 0.01 M NaCl, mixed with pre-conditioned H^+ resin (≈5–10 × wt. of PLCNFs), and stirred for 1 h at room temperature. Then, the resin was removed and the suspension washed with water. The protonated suspension was afterwards titrated potentiometrically with standardized NaOH (0.05 M) from pH 2 to pH 11 while recording the conductivity and the pH versus added volume. Equivalence volumes were determined by derivative/Gran analysis, and the total charge was calculated from the net NaOH consumption normalized to dry mass (Eq. (1)). Experiments were performed in triplicate to ensure reproducibility.

$$C_{charge}(mmol/g) = \frac{M_{NaOH} \times V_{NaOH} \times 1000}{m_{sample(g)}} \qquad (1)$$

where M_{NaOH}, V_{NaOH}, and m_{sample} correspond to the molarity of NaOH solution in $mol.L^{-1}$, volume of NaOH in L corresponding to the second inflection point, and weight of the PLCNF sample in g, respectively.

The chemical composition of PLCNFs was determined according to TAPPI standard protocols (TAPPI T 257cm-02), including Tappi T222 om-88 for Klason lignin, Tappi T249-cm-85 for hemicellulose, and TAPPI 429 om-23 for cellulose content.

FTIR analysis of the films was performed using attenuated total reflectance (ATR) mode in a Perkin-Elmer 2000 spectrometer. The absorbance spectra were recorded within the wavenumber range of 600–4000 cm^{-1}, with a spectral resolution of 4 cm^{-1} and an accumulation of 16 scans at room temperature. All measurements were conducted in triplicate.

The transmittance of the neat and composite films was evaluated using a UV–Vis spectrophotometer (Lambda 35, PerkinElmer, Waltham, MA, USA) operating within the wavelength range of 200–800 nm. Measurements were performed in triplicate.

The washability of the neat and composite films was assessed over three consecutive washing-drying cycles. The films (2 cm × 2 cm) were initially dried at 50 °C to a constant mass ($m_{0,\ dry}$). Each sample was then immersed in 50 mL of deionized water for 30 min at room temperature. The swollen films were gently removed, and the surface was blot-dried with filter paper. The films were subsequently re-dried at 50 °C until constant mass and weighed again ($m_{n,\ dry}$). The procedure was repeated for three cycles (n = 1, 2, 3). The mass retention (MR_n) was calculated for each cycle based on the following equations:

$$MR_n(\%) = \frac{m_{n,\ dry}}{m_{0,\ dry}} \times 100 \qquad (2)$$

Differential scanning calorimetry (DSC) thermograms were recorded under a nitrogen atmosphere using a Perkin-Elmer differential scanning calorimeter. Approximately 4–6 mg of the sample was hermetically sealed in an aluminum pan, and the sample was subjected to a first heating scan from 20 to 230 °C at a rate of 10 °C.min^{-1}, followed by a cooling scan at the same cooling rate. The degree of crystallinity (X_c) was calculated using Eq. (3):

$$X_c = \frac{\Delta H_m}{\Delta H^0{}_m \times W_{PVA}} \times 100 \qquad (3)$$

where ΔH_m is the enthalpy of fusion, $\Delta H°_m$ is the theoretical enthalpy of fusion of 100 % crystalline PVA (138.7 J.g^{-1}), and W_{PVA} is the weight fraction of PVA in the composite.

Thermogravimetric analysis (TGA) was performed using a PerkinElmer TGA 400 analyzer on samples of approximately 10 mg, over a temperature range of 50 to 700 °C, at a constant heating rate of 10 °C.min^{-1}. To investigate thermal stability and decomposition mechanisms, measurements were conducted independently under air and nitrogen atmospheres.

The combustion behavior of the films was evaluated using a Microscale Combustion Calorimeter (MCC, Fire Testing Technology Ltd., UK), in accordance with ASTM D7309. Samples (~10 mg) were pyrolyzed under nitrogen at a controlled heating rate of 1 °C.s^{-1} up to 700 °C. The volatile products were combusted at 900 °C under a continuous N_2/O_2 flow (80 mL.min^{-1}/20 mL.min^{-1}). Key parameters, including heat release rate (HRR), peak of heat release (PHRR), total heat release (THR), heat release capacity (HRC), and final residue, were recorded. All measurements were performed in triplicate.

Water contact angle (WCA) was measured using a Dataphysics OCA 15 Drop Shape Analyzer, equipped with a high-resolution CCD camera, operating at an acquisition rate of 50 images per second. A water droplet was deposited on the surface of the thin films. The data were analyzed using OCA software.

For the moisture sorption, square films (5 × 5 cm^2) were dried at 90 °C for 4 h, then stored in a desiccator with saturated salt solutions (NaCl for 75 % RH, and $Mg(NO_3)_2$ for 55 % RH) to ensure controlled humidity conditions. Moisture uptake was monitored by recording the change in sample mass over time. The moisture sorption capacity was calculated using the following equation:

$$Moisture\ sorption(\%) = \frac{(m_t - m_0)}{(m_0)} \times 100 \qquad (4)$$

where m_0 is the initial weight of the dry sample and m_t *is* the weight of the sample at a given time, respectively.

Dynamic mechanical analysis (DMA) was performed in tension mode using PYRISTM Diamond DMA (Perkin-Elmer, Waltham, MA) under heating at 2 °C min^{-1}, at a vibration

frequency of 1 Hz. The storage (E') and loss (E“) moduli were measured as a function of temperature.

The tensile test was performed using a Universal Testing Machine (TM2101 V4.23) equipped with a 500 N load cell. Experiments were performed at room temperature at a rate of 10 mm min^{-1}. The specimens were cut into rectangular strips measuring 5 mm in width and 30 mm in length, with a thickness range of 58–86 μm.

3. Results and discussion

3.1. Characterization of PLCNFs

Cellulose nanomaterials are highly appealing for composite applications due to their outstanding strength and stiffness, reported to be 2–6 GPa and 150 GPa, respectively [22,23]. Their high surface area, aspect ratio, and ability to form networks through hydrogen bonding and secondary interactions further enhance the mechanical performance of these bio-based constituents. However, their low moisture resistance remains a limitation. To address this and enhance composite properties, we produced lignin-cellulose nanofibrils herein via a green phosphorylation approach. The resulting PLCNFs consist of cellulose (59.2 %), hemicellulose (18.7 %), and lignin (22.1 %) with a yield of 60 % ($m_{PLCNF}/m_{Giant\ reed}$). Unlike hydrophilic cellulose, lignin is relatively hydrophobic, contributing to water resistance similar to natural plant systems. Hemicellulose facilitates the coexistence of cellulose and lignin in the PLCNF suspension by acting as a compatibilizing agent. Following phosphorylation and alkali-swelling, the charge content of PLCNFs reached C_{charge} = 6100 mmol.kg^{-1}, which promoted the mechanical disintegration of the phosphorylated giant reed into nanomaterials through electrostatic repulsion among negatively charged fibrils.

It is worth noting that the conversion of phosphorylated native Arundo donax (giant reed) biomass into nanoscale phosphorylated lignocellulosic nanofibrils (PLCNFs) was achieved through a single pass in a microfluidizer. This process resulted in the formation of a thick, yellowish, translucent gel **(**Fig. 1a**)**. Transmission electron microscopy (TEM) analysis of the diluted PLCNF suspension **(**Fig. 1**)** revealed individual, slender nanofibrils forming an entangled network, with an average fibril width of 4.5 ± 0.6 nm. Additionally, spherical particles with diameters ranging from 10 to 20 nm, observed in the magnified TEM images (indicated by red arrows), are likely lignin nanoparticles coexisting with the cellulose nanofibrils in the suspension. The efficient fibrillation of the giant reed biomass into PLCNFs is attributed to the high density of introduced ionic phosphate groups, which intensify osmotic pressure, capillary suction, and internal electrostatic repulsion forces. These combined effects are sufficient to overcome the intrinsic cohesion of the lignocellulosic fiber network. Similar

behavior has been reported for other chemically modified cellulose or lignocellulosic materials, including those subjected to TEMPO-mediated oxidation, periodate oxidation followed by amination, sulfation, and cationization, where spontaneous nanofibrillation and gel formation occur when the ionic group content exceeds a critical threshold [24].

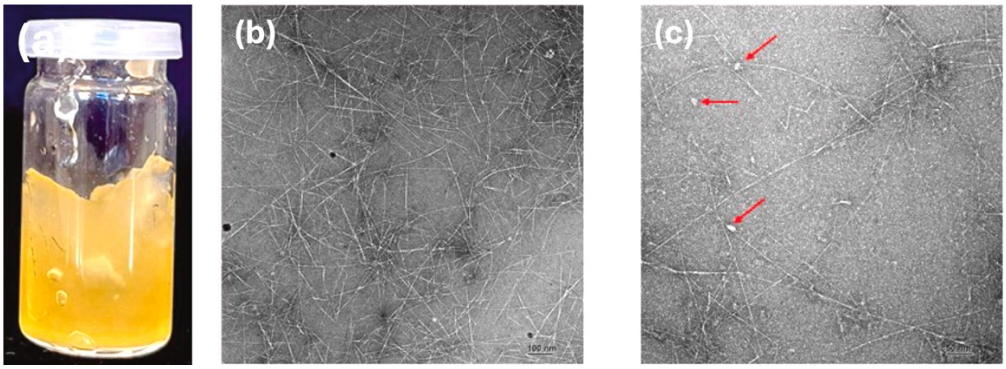

Fig. 1. (a) Visual aspect of the PLCNF gel, and (b, c) TEM images of PLCNF suspension at different magnifications.

3.2. Characterization of PVA/PLCNF composite films

CNFs have been widely incorporated into various polymer matrices to impart specific properties such as mechanical reinforcement, barrier performance, and antibacterial activity [25], [26], [27]. Since these properties are strongly influenced by the CNF content and their degree of dispersion within the polymer matrix, selecting a waterborne polymer dispersion or a water-soluble polymer is an efficient strategy to prevent nanocellulose aggregation during the nanocomposite processing. Accordingly, PVA was chosen as the polymer matrix in this work, and films were prepared via the solvent casting method. Biocomposites containing up to 20 wt% PLCNF were prepared, and the effect of PLCNF loading on their thermal, mechanical, and UV-shielding properties was investigated.

3.2.1. UV-absorption and structural analysis

Lignin-based materials such as LCNF contain functional phenolic and carbonyl groups that enable them to serve as effective UV-absorbing moieties in polymer nanocomposites intended for packaging and protective film applications [28]. To evaluate the UV-shielding capacity of the PLCNFs, UV–Vis transmittance spectra were recorded for the neat PLCNF, neat PVA, and PVA/PLCNF composite films across the 200–800 nm range **(**Fig. 2a**).** The transparent, neat PVA film showed no significant absorption across the UV–Vis range, with a transmittance exceeding 80 % between 400 and 800 nm, indicating high optical transparency. In contrast, the PLCNF film appeared slightly brown in color and exhibited nearly total absorption in the UV region (200–350 nm), with a moderate transmittance of ~35 % in the visible region. This

reflects the strong UV-blocking ability of the PLCNFs, likely attributed to its high residual lignin content. The presence of chromophore moieties in the guaiacyl structure of lignin enables UV light absorption, converting it into heat or other forms of energy, thereby preventing it from reaching the polymer matrix [29,30]. In the composite film, efficient UV absorption was achieved at PLCNF contents above 10 wt%, with more than 80 % of the UV light absorbed. However, the strong UV-absorbing properties are accompanied by a reduction in film transparency, as evidenced by the progressive decrease in the transmittance with increasing PLCNF content. This reduction in transparency is likely attributed to the presence of large lignin particles (>100 nm), which promote light scattering and consequently reduce the amount of transmitted light [31]. The decline in transparency of the composite films is also visually evident in the photographs, where the background images become progressively less visible as the PLCNF content increases to 20 wt% **(**Fig. SI3**).**

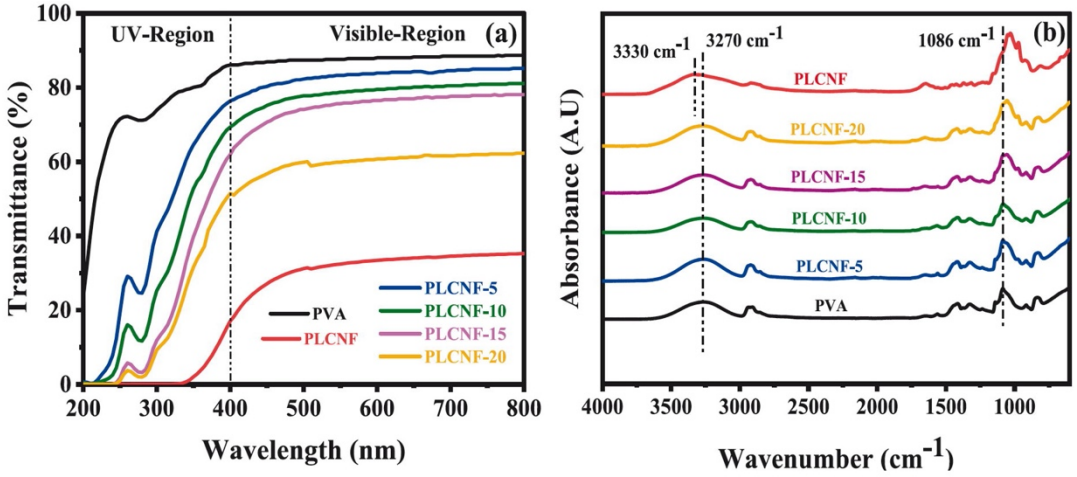

Fig. 2. (a) UV-transmittance, (b) FTIR spectra of neat PVA, PLCNF, and PVA/PLCNF composite films with different PLCNF concentrations (0, 5, 10, 15, and 20 wt%).

The structure of the PLCNFs and PVA/PLCNF composites was investigated by ATR-FTIR spectroscopy **(**Fig. 2b**)**. PLCNFs, PVA, and their composite films exhibited stretching vibration peaks of hydroxyl groups (O–H) at around 3330 cm^{-1} and 3270 cm^{-1}, respectively. Remarkably, increasing the PLCNF loading in PVA resulted in a gradual shift of the O–H stretching vibration in the nanocomposite films, from 3260 cm^{-1} for PLCNF-5 to 3300 cm^{-1} for PLCNF-20. Meanwhile, the C-OH peak position progressively shifted from 1086 cm^{-1} to 1054 cm^{-1} as the PLCNF loading increased to 20 wt% in the PVA nanocomposite film. These peak shifts can be attributed to the formation of intermolecular hydrogen bonds between the functional groups on the PLCNFs and the hydroxyl groups of PVA [19]. Notably, the high content of phosphate functional groups on the surface of PLCNFs led to improved dispersion

and promoted the formation of hydrogen bonds between the hydroxyl groups of PLCNFs and PVA, enhancing interfacial interactions within the composite films.

3.2.2. Morphology characterization of the composites

The cross-section SEM images presented in Fig. 3 illustrate the morphological changes in the films with increasing PLCNF content. The neat PVA film **(**Fig. 3a**)** shows a relatively smooth and dense cross-section, characteristic of a homogeneous polymeric matrix. The incorporation of 5 wt% PLCNF **(**Fig. 3b**)** reveals slight heterogeneity and interfacial fracture-related irregularities, suggesting poor dispersion and weak matrix-filler interactions at low filler content. At 10 and 15 wt% PLCNF **(**Fig. 3**)**, the cross-sections exhibit an increasingly rough and textured appearance, indicating improved integration of the nanofibrils within the matrix and a compact structure. This enhancement is likely attributed to stronger interfacial adhesion and hydrogen bonding between PVA and PLCNFs. The 20 wt% composite **(**Fig. 3e**)** shows a highly compact morphology, with visible irregularities, suggesting the formation of a well-structured hybrid network.

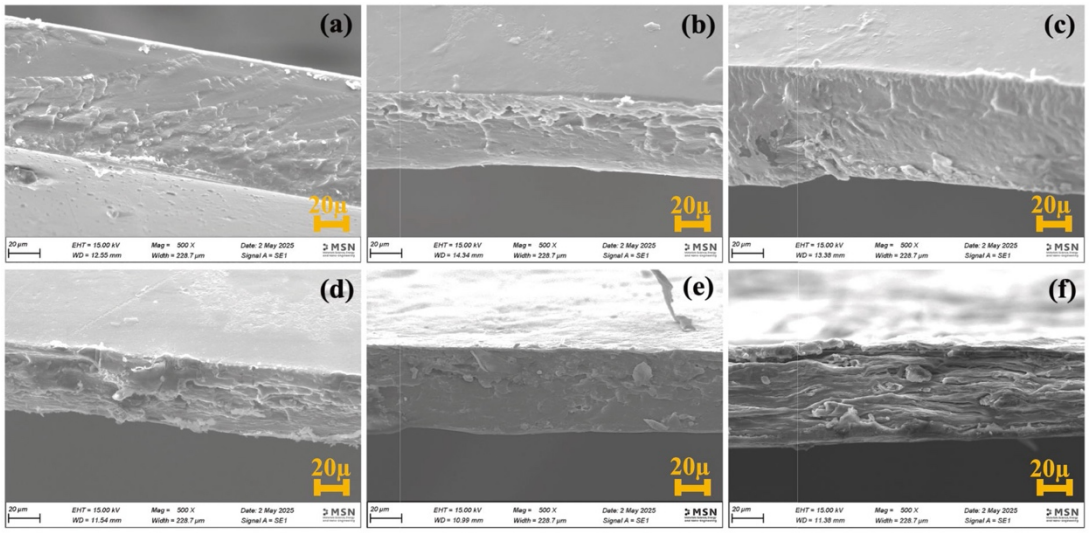

Fig. 3. SEM images of cryo-fractured cross-section of (a) neat PVA, (b) PLCNF-5, (c) PLCNF-10, (d) PLCNF-15, (e) PLCNF-20, and (f) PLCNF films.

The neat PLCNF film **(**Fig. 3f**)** displays a fully fibrillar structure, with a densely stacked and layered fibrillar morphology typical of nanocellulose-based networks. In this case, the absence of a polymer matrix led to a highly oriented and uneven surface morphology, characterized by visible fibril stacking that reflects strong interfibrillar interactions. These observations suggest that higher PLCNF content improves structural integrity, attributed to enhanced network formation and interfacial bonding.

3.2.3. Washability of the films

The washability of the neat and composite films was evaluated over three sequential washing-drying cycles by tracking the residual dry mass after each cycle **(**Table 1**).** Neat PVA exhibited noticeable mass loss after the first cycle, with final mass retention stabilizing at 77.2 % after the third cycle, which confirms partial dissolution during water exposure. PVA/PLCNF composite films retained most of their initial mass through the cycles. The final mass retention ranged from ~79 to ~85 %, with PLCNF-20 showing the highest stability after the last cycle (84.7 %). The neat PLCNF film showed lower retention (69.5 %) after the third cycle, highlighting the importance of incorporating PLCNFs into the PVA matrix to ensure better cohesion and water resistance. The strong interfacial bonding between PVA and PLCNFs, combined with the lignin-induced hydrophobic nature of the nanofibrils, effectively limited polymer leaching and enabled good structural recovery after redrying. Additionally, visible morphological changes were observed. The neat PVA film experienced major shrinkage due to its hydrophilic nature, whereas the incorporation of PLCNFs reduced its hydrophilicity, as supported by the contact angle results, and led to a more compact structure (Fig. SI4). The enhanced network of hydrogen bonds between the filler and the matrix prevented excessive shrinkage upon drying and minimized mass loss over repeated washing cycles, resulting in improved durability compared to neat PVA. The possibility of chemical interaction between PLCNF and PVA, via chemical condensation of the hydroxyl group of PVA and grafted phosphate to form a phosphate ester bond, is another possibility that may be considered. Indeed, from the chemical point of view, this reaction is possible and widely observed in living cells. Overall, the composite films with high PLCNF content maintained a cohesive structure after water rinsing and air-drying, confirming their stable washability performance.

Table 1. Mass retention of neat and composite films over three washing-drying cycles.

Sample	Mass retention after cycle 1 (%)	Mass retention after cycle 2 (%)	Mass retention after cycle 3 (%)
PVA	79.3	77.9	77.2
PLCNF-5	84.4	82.6	79.7
PLCNF-10	85.5	83.9	82.2
PLCNF-15	86.3	84.8	83.2
PLCNF-20	87.7	85.3	84.7
PLCNF	73.3	72.9	69.5

3.2.4. Thermal properties

DSC analysis of the composite samples was performed to investigate how the addition of the PLCNF nanofiller affects the thermal transition of the PVA matrix. The DSC profiles of the cooling and heating processes for PLCNFs, PVA, and their composite films are presented in Fig. 4. During the first heating scan, neat PVA exhibits a melting peak at 222 °C, while a crystallization peak appears at 200 °C during the cooling scan. Upon incorporation of PLCNFs, the melting peak shifts to approximately 230 °C across all composite films, and the crystallization temperature increases to around 207–209 °C, depending on the PLCNF content. This upward shift in the melting temperature is likely attributed to the hydrogen bonding between PLCNFs and PVA, which restricts chain mobility and makes the PVA crystallites more difficult to melt.

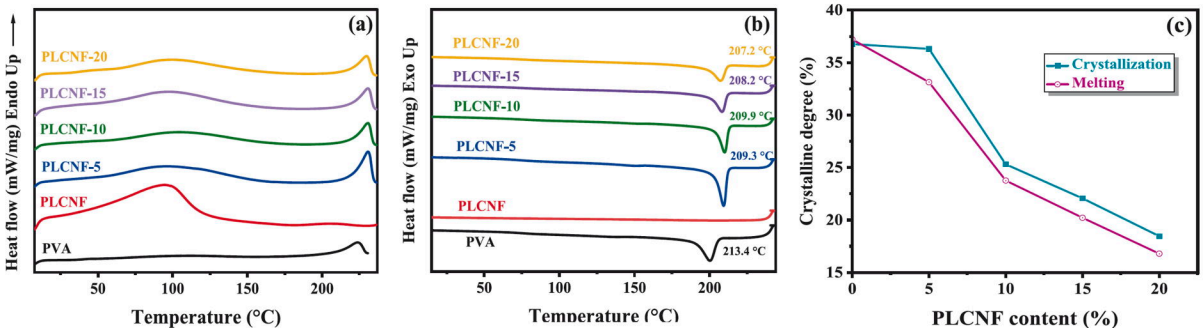

Fig. 4. (a, b) DSC curves of PLCNFs and PVA/PLCNF composite films with different PLCNF loadings (0, 5, 10, 15, and 20%) under an air atmosphere, and (c) crystalline degree (%) of nanocomposite films as a function of PLCNF content.

In addition to thermal transitions, the incorporation of PLCNFs also influences the crystallinity degree (X_c) of the PVA matrix. As shown in Fig. 4c, X_c decreases progressively with increasing PLCNF content, from ~36 % in neat PVA to about 18 % at 20 wt% PLCNF. This reduction in X_c suggests that PLCNFs hinder the crystallization of PVA chains, likely due to the strong hydrogen bonding between PLCNFs and PVA, which disrupts the regular packing of PVA chains into the crystalline lattices. A similar tendency was reported for PVA composite based on CNF nanofiller [1].

TGA measurements were conducted on PLCNFs, PVA, and their composites to evaluate their thermal behavior under both air and nitrogen atmospheres. TGA/DTG curves are shown in Fig. 5. Key thermal parameters, including the temperature at 50 % weight loss ($T_{50\%}$), the temperature of maximum degradation (T_{max}), and the solid residue at 800 °C, are summarized in Table 1. Three distinct thermal decomposition steps were observed for both neat films and all PVA/PLCNF composites under nitrogen. The initial minor weight loss observed below

100 °C is attributed to the evaporation of moisture. This weight loss increased with higher PLCNF loadings and was most pronounced in the neat PLCNF film, likely due to the presence of OH groups introduced by phosphate functionalities during phosphorylation, which enhances the hygroscopic nature of PLCNFs. In neat PLCNF film, a second mass loss occurred between 230 °C and 350 °C, corresponding to the degradation of hemicellulose and cellulose molecular side chains. This process includes the cleavage of glycosidic bonds, dehydration, and depolymerization of glycosidic rings [11]. The high T_{max} (325.1 °C) and char residue (32.4 %) of PLCNFs can be attributed to the high thermal stability of lignin, which is characterized by its aromatic structure and high degree of branching [30]. It is noteworthy that the high phosphorus content in PLCNFs also contributes to a lower onset of thermal degradation and increases char yield. A similar trend was reported for phosphorylated lignin-free CNFs, where phosphate groups lowered the onset temperature from 248.10 to 178.92 °C [32]. The thermal decomposition of neat PVA film occurred between 200 °C and 500 °C, with a T_{max} of 274.1 °C and a low char residue of 3.3 % at 800 °C **(**Table 2**)**. The T_{max} of the PVA/PLCNF composites shifted to higher values with the increasing PLCNF loading compared to neat PVA. For instance, the incorporation of 5 wt% PLCNF increased T_{max} to 281.2 °C, compared to 274.1 °C for neat PVA. At 20 wt% PLCNF loading, T_{max} increased significantly to 351.8 °C, indicating a substantial enhancement in thermal stability. This improvement can be attributed to the inherent high thermal stability of lignin and the intermolecular interactions between the nanofillers and the PVA matrix [19]. Furthermore, $T_{50\%}$values increased with PLCNF content, reflecting delayed decomposition under inert conditions. This delay occurred during the second degradation stage, observed below 400 °C, which is attributed to the decomposition of PVA side chains and the overlapping thermal degradation of lignin and cellulose. The third degradation stage, observed between 400 and 500 °C, corresponds to the degradation of the PVA backbone [30]. Char residue also increased significantly with higher PLCNF loading, reaching 11.8 % at 800 °C for the composite with 20 wt% PLCNF, confirming the char-forming nature of lignin/phosphate and the thermal stability of the phosphorylated nanofibrils under nitrogen.

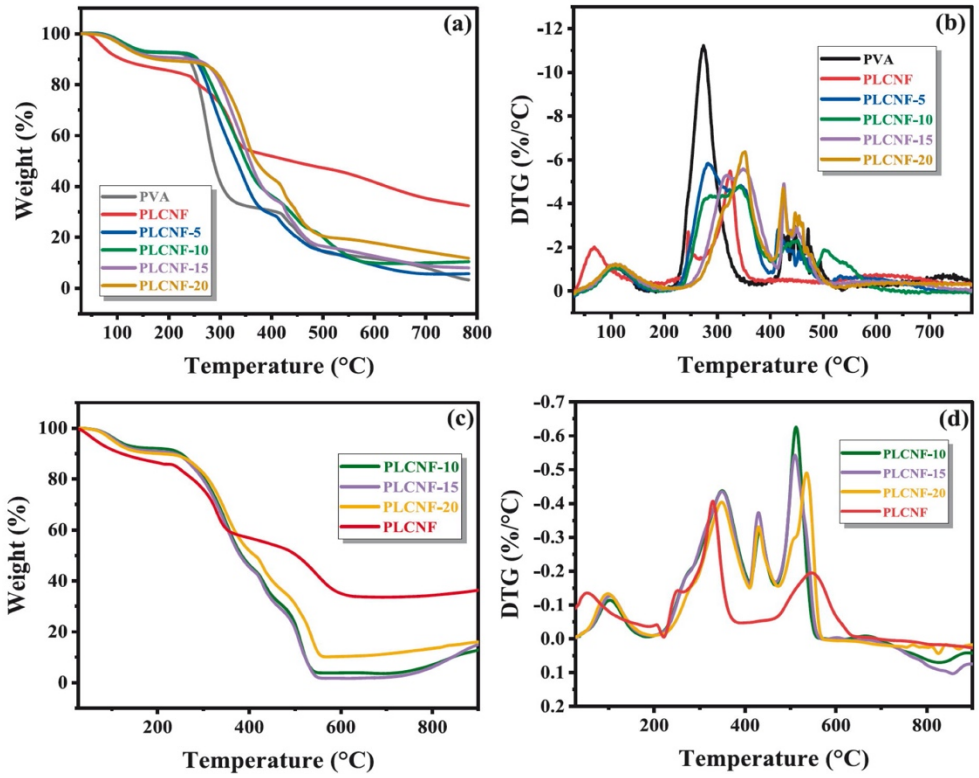

Fig. 5. (a) TGA curves and (b) the corresponding DTG curves under N_2, (c) TGA curves, and (d) DTG curves under air of PLCNF and PVA/PLCNF composite films with different PLCNF loadings (0, 5, 10, 15, and 20 wt%).

Table 2. TGA and DTG data for PVA, PLCNFs, and PVA/PLCNF composites.

	Under N_2			Under Air		
Sample	**$T_{50\%}$(°C)[a]**	**T_{max}(°C)[b]**	**Char residue at 800 °C (%)**	**$T_{50\%}$(°C)[a]**	**T_{max}(°C)[a]**	**Char residue at 900 °C (%)**
PVA	287.6	274.1	3.3	287.6	–	–
PLCNF-5	331.3	281.2	5.7	331.3	–	–
PLCNF-10	349.1	343.3	10.4	349.1	513.3	12.5
PLCNF-15	358.7	349.6	8	358.7	508.6	14.9
PLCNF-20	370.7	351.8	11.8	370.7	534.9	15.8
PLCNF	430.4	325.1	32.4	430.4	547.5	36.4

[a] $T_{50\%}$: the temperature at 50% mass loss.
[b] T_{max}: Temperature at maximum decomposition rate.

Under oxidative atmospheres, thermal degradation occurred at higher temperatures, resulting in sharper DTG peaks. Moreover, composites with higher PLCNF content exhibited higher solid residue than neat PVA. These findings confirm that PLCNFs enhance the thermal stability of PVA/PLCNF composites and promote char formation during decomposition, presumably due to the conversion of lignin into a thermally stable char under oxidative conditions [19,33].

3.2.5. Flame retardancy

Microscale combustion calorimetry (MCC) tests were conducted to investigate the flame retardancy of neat and composite films. MCC is a rapid and effective technique for quantitatively assessing the burning behavior and fire hazard of polymeric materials. This testing method evaluates the thermal combustion behavior of small-scale samples, providing insights into heat release behavior and combustion properties. However, it does not capture bulk combustion phenomena [34,35]. The heat release rate (HRR) curves are presented in Fig. 6a. The flammability parameters, including THR, PHRR, and HRC, are summarized in Table 3.

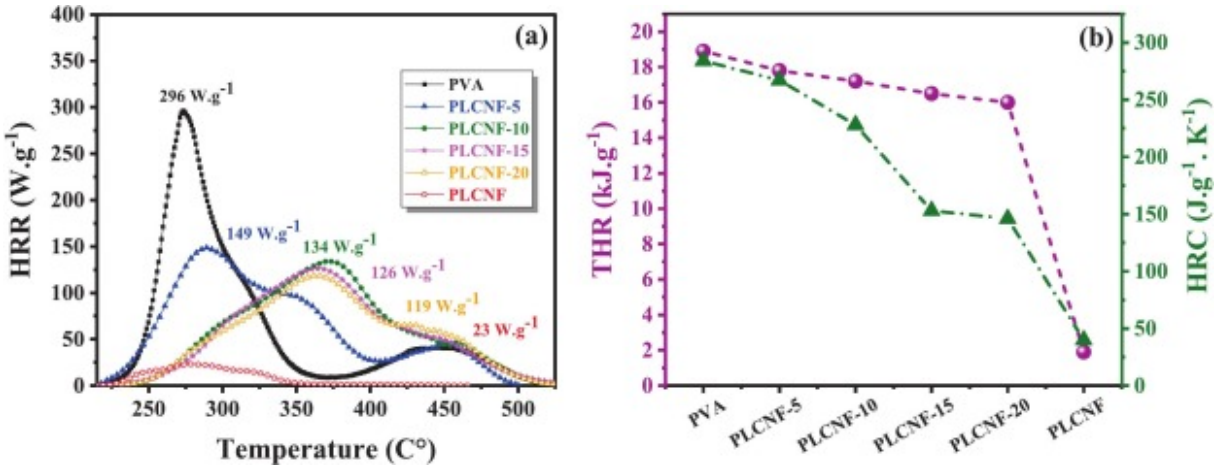

Fig. 6. (a) HRR vs. temperature curves and (b) THR of PVA, PLCNFs, and PVA/PLCNF films from the MCC test.

Table 3. Microscale combustion calorimeter (MCC) data for the different film samples.

Sample	PHRR ($W.g^{-1}$)[a]	THR ($kJ.g^{-1}$)[b]	HRC ($J.g^{-1}.K^{-1}$)[c]
PVA	296	18.9	284
PLCNF-5	149	17.8	267
PLCNF-10	134	17.2	228
PLCNF-15	126	16.5	153
PLCNF-20	119	16	146
PLCNF	23	1.9	40

[a] PHRR: Peak heat release rate; [b] THR: Total heat release; [c] HRC: Heat release capacity.

Neat PVA film exhibited a narrow HRR peak at 273.2°C, followed by a minor broad peak at 446.4°C, indicating a two-stage degradation process. Similarly, the HRR curve of neat PLCNF film exhibited two broad and overlapping peaks at 276.3 °C and 316.1 °C, indicating the formation of char through cellulose and lignin oxidation/dehydration at elevated

temperatures [36]. This behavior suggests a synergistic flame-retardant effect between lignin and phosphorus [33]. All PVA/PLCNF composites demonstrated distinct HRR patterns, characterized by a three-stage decomposition process. Increasing PLCNF content shifted the HRR peaks towards higher temperatures, indicating a delay in the combustion process. The composites exhibited a significant reduction in heat release, with broad overlapped peaks at lower temperatures and minimal heat release around 450 °C. At 20 wt% PLCNF, PHRR and THR were reduced by ~60 % and ~15.3 %, respectively, while HRC decreased by ~48.6 %, highlighting the effectiveness of PLCNFs in improving the flame retardancy **(**Fig. 6b**)**. The reduction in PHRR at high PLCNF loading directly correlates with the increase in char residue, confirming the contributions of phosphorus and lignin to the improved flame-retardant efficiency.

The flame-retardant performance of PLCNFs can be attributed to the complementary actions of phosphate groups and lignin in both the gas and condensed phases. During combustion, cellulose chains and lignin are carbonized to form a layer containing P_xO_y and a carbon layer that redeposits on the film surface [37].The flammable volatiles resulting from the degradation of the polymer matrix participate in combustion reactions with oxygen in air, releasing free radicals (H• and HO•) and heat. The presence of phosphorus interrupts the combustion process, where the released PO• free radicals react with highly active H• and HO• free radicals, which promotes dehydration, resulting in the formation of char [38]. Simultaneously, lignin further contributes to char formation. Lignin is a thermally stable biopolymer that exhibits outstanding char-forming capability at elevated temperatures due to its aromatic structure. The cleavage of functional groups and the rearrangement of the polymer backbone at higher temperatures can lead to the formation of high char residues, which effectively prevent heat and mass transfer between the condensed and the gas phases [33]. The generated protective layer provides an effective physical barrier against heat and oxygen diffusion for the underlying polymer, suppressing further combustion and resulting in an evidently improved flame resistance of the composite films, while the release of non-flammable gases (e.g., CO, CO_2, H_2O) dilutes combustible volatiles in the combustion zone [39,40]. The combination of condensed and gas-phase mechanisms effectively inhibits heat release and flame propagation, which is consistent with the reduced PHRR and THR observed in MCC testing. A schematic representation of this mechanism is illustrated in **(**Fig. 7**).**Therefore, it can be said that the synergistic flame-retardant effect of phosphorus-containing groups and lignin efficiently limits cellulose chain degradation during the combustion process.

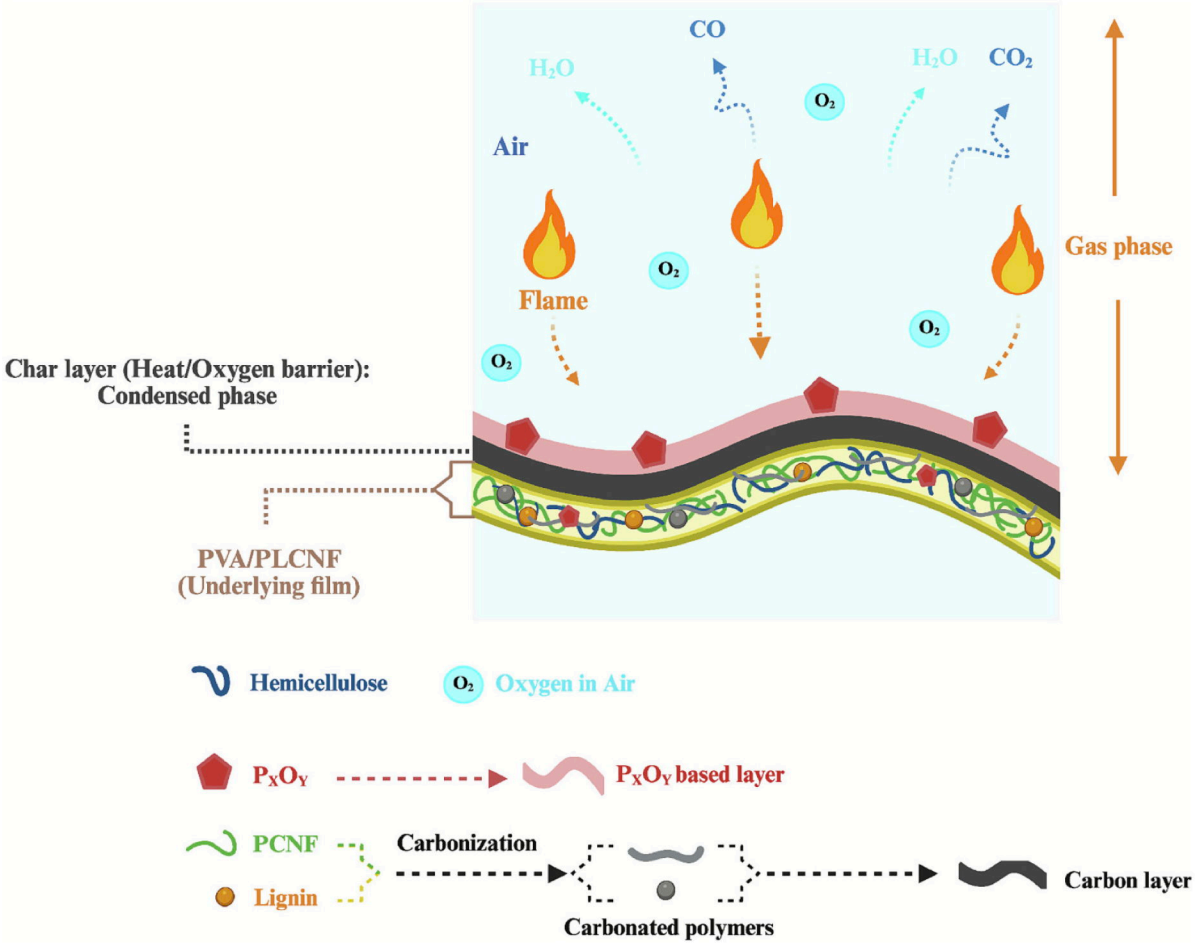

Fig. 7. The proposed synergistic flame-retardant mechanism of lignin and phosphate groups in PLCNF$_S$.

The combustion behavior of the neat and composite films was further investigated via a vertical burning test. Film strips of 1 cm × 3 cm were exposed to a flame source **(**Fig. 8**).** The neat PVA film ignited quickly and burned with rapid upward flame spread, leading to a significantly short combustion time (<10 s) and quick shrinkage under heat exposure, accompanied by a noticeable amount of smoke. Almost the entire film was consumed, leaving only a very small and brittle residue after combustion.

In contrast, the PVA/PLCNF composite films curled up and exhibited a more controlled, slower flame spread compared to the neat PVA film, indicating improved burning behavior. The presence of PLCNFs promoted the formation of a char layer, which served as a physical barrier, restricting heat transfer and delaying degradation. As a result, the flame height was noticeably reduced with increasing PLCNF content, and the flame self-extinguished shortly after the removal of the ignition source, with slight fume generation compared to the neat PVA film. Moreover, a substantially larger amount of char residue was retained, and the remaining structure appeared swollen and expanded, suggesting the development of an insulating char barrier.

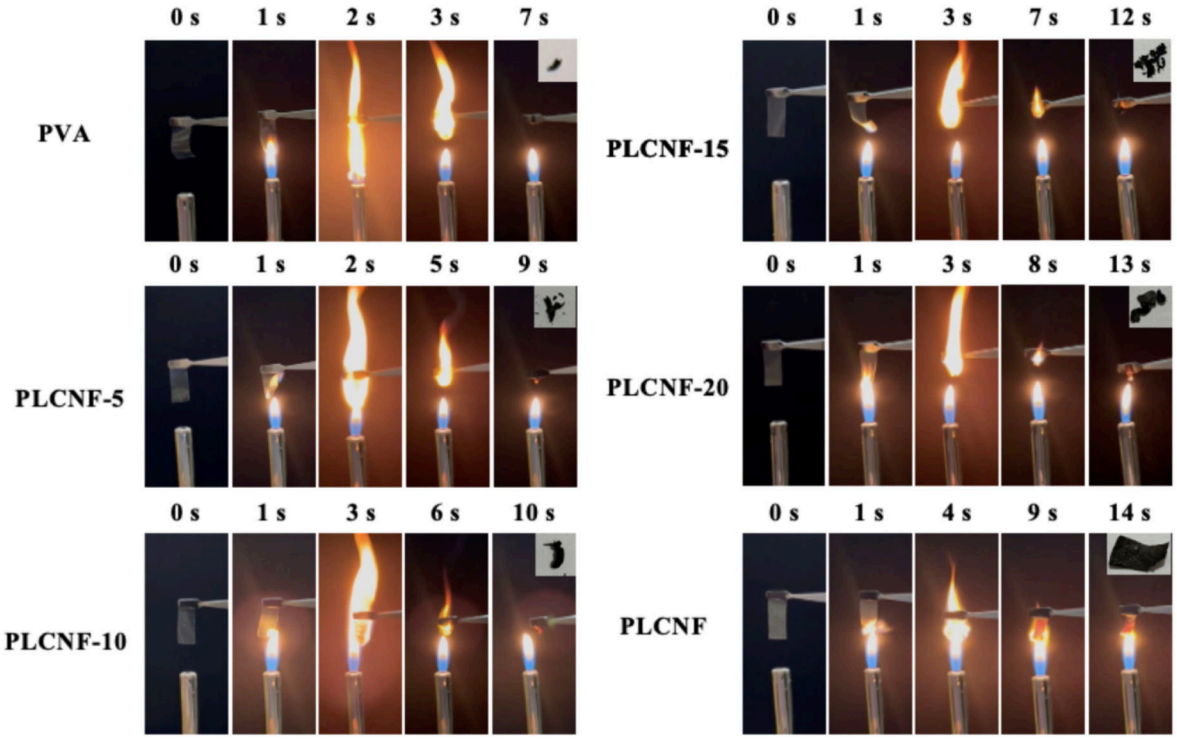

Fig. 8. Vertical burning test of PVA, PLCNF, and PVA/PLCNF films.

Although the neat PLCNF film still ignited, the flame propagated more slowly. In this case, the strip rapidly swelled after the flame exposure and retained better structural integrity during combustion. A more cohesive and protective char layer formed, which resisted further burning, resulting in a longer burning duration (>10 s) and slower flame propagation, with very limited smoke release compared to neat PVA and composite films. These observations confirm that incorporating PLCNFs enhances the flame resistance of PVA by promoting char formation and limiting the combustion process, which is consistent with the MCC results.

3.2.6. Contact angle and moisture uptake

The surface wettability of the neat PLCNF film and PVA/PLCNF composite films was evaluated using optical contact angle (CA) measurements to assess the effect of PLCNF content on their hydrophilic/hydrophobic properties **(**Fig. 9a**)**. The neat PVA film exhibited a contact angle of approximately 41°, indicating a hydrophilic surface. As the PLCNF content increased, the CA rose to around 49° and 53° for films containing 15 and 20 wt% PLCNF (PLCNF-15 and PLCNF-20), respectively. Although the increase in water contact angle is moderate, it suggests a reduction in the hydrophilic character of the composite films with higher PLCNF loading. This effect is likely due to the presence of lignin in PLCNFs, which is known to impart hydrophobic properties. This also explains the relatively high CA of the neat PLCNF film (without PVA), which showed a contact angle of approximately 83°. A similar trend was

reported by Zhang et al. [19], which showed that incorporating oxidized lignocellulosic nanofibrils (t-LCNF) into PVA enhanced the hydrophobicity of the resulting composite films, achieving a contact angle of 97.3° at 20 wt% t-LCNF, indicating reduced wettability.

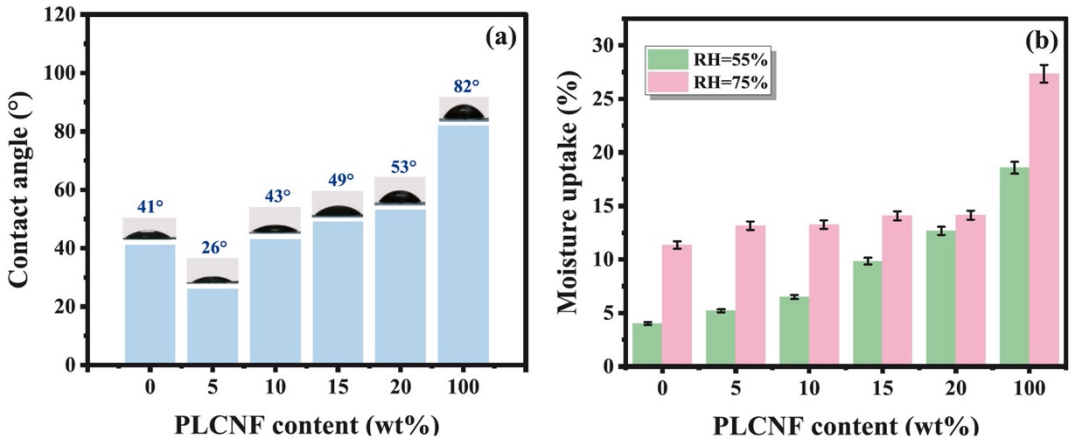

Fig. 9. (a) Contact angle and (b) moisture uptake of neat PVA, PLCNF, and PVA/PLCNF films with different PLCNF loadings exposed to controlled humidity environments of 55 and 75% RH.

Moisture uptake behavior of pristine PLCNF film and its composite films was examined under controlled relative humidity (RH) conditions of 55 % and 75 % **(**Fig. 9b**)**. PLCNFs exhibited a higher moisture uptake compared to the neat PVA matrix. As the PLCNF content increased, a gradual rise in moisture uptake was observed in all composite films, indicating greater susceptibility to water absorption with higher PLCNF loading. At 55 % RH, the composite films exhibited a gradual increase in the moisture uptake with the increasing PLCNF content. Nevertheless, at 75 % RH, the composites showed moisture uptake values comparable to those of neat PVA, suggesting strong matrix-filler interactions that suppress moisture uptake under higher humidity conditions. Despite the presence of a relatively high amount of residual lignin, known to be hydrophobic, the PLCNFs demonstrated a high tendency to absorb moisture, presumably due to the high density of phosphate and phosphoric groups. These marked hydrophilic properties of PLCNFs justify the increase in moisture uptake as their content increases. This effect became more pronounced when the film was exposed to high relative humidity, where moisture uptake exceeding 14 % was achieved for composite films with a PLCNF content over 15 wt%.

These findings reveal that different mechanisms govern contact angle and moisture uptake. While the contact angle increases with PLCNF content, indicating surface hydrophobicity, the bulk moisture uptake does not follow the same trend. This discrepancy highlights the complex interplay between surface chemistry and matrix-filler interactions in determining moisture behavior, with the co-existing lignin and phosphate groups in PLCNFs being key contributors.

Lignin imparts hydrophobicity, whereas the charged phosphate groups increase hydrophilicity, resulting in opposing effects on surface wettability.

3.2.7. Mechanical properties

The effect of PLCNF incorporation on the mechanical performance of PVA films was evaluated through stress–strain analysis and DMA **(**Fig. 10**)**. The addition of PLCNFs induced a steady increase in both tensile modulus (E) and ultimate strength (US) **(**Table 4**)**, reflecting the strong reinforcing capacity of PLCNFs. For instance, E and US increased from 1.2 GPa and 34 MPa for neat PVA to 2.2 GPa and 58 MPa at 10 wt% PLCNF content and reached 2.9 GPa and 95 MPa at 20 wt% PLCNF content, respectively. Neat PLCNF film exhibited the highest stiffness (3.8 GPa) and a tensile strength of 90 MPa, as expected for a matrix-free, nanofibril-dominated structure. Mechanical properties of CNF film (also termed nanopaper) have been widely discussed in the literature, and are widely dependent on the cellulose molar mass, on the nanopaper porosity, and on the degree of fibril alignment in the nanopaper. Values up to 33 GPa and 400 MPa have been registered for samples with oriented fibrils [41], while values around 10 GPa and 200 MPa are expected for samples with random orientation [42,43]. Hence, the values of PLCNF film obtained herein are lower, probably due to lignin presence hindering the nanofibrillar network, and impeding plastic deformation. Consequently, the PLCNF film registers a lower strain to failure of only 3.3 % equivalent to a work-to-fracture of 2.1 $MJ.m^{-3}$. Yet, the reinforcing and toughening potential of PLCNFs is excellent, and aligns with the compact and interconnected morphology observed in SEM, where the fibrillar network promotes efficient stress transfer, and the lignin acts as a compatibilizer with the PVA matrix. This structural reinforcement explains the observed increase in E and US. As for the US, the yield strength increases with the addition of PLCNFs to PVA **(**Table 4**)**, going from 22.3 MPa for PVA to 54.7 MPa for PLCNF-20. Interestingly, the ductility of the composites shows an unusual behavior, where the strain at break and strain at maximum stress are higher for some composites as compared to the neat PVA. The PLCNF-10 composite, for example, registers a strain at break of 49 % translating into an outstanding work-to-fracture of 30 $MJ.m^{-3}$, which is nearly an order of magnitude higher than the value of the neat PVA and neat PLCNF films. High toughness is important for advanced composite applications, balancing stiffness, strength, and energy-dissipation mechanisms. Here, crack deflection by the CNF network, as well as stiff CNF combination with soft and ductile PVA matrix, are responsible mechanisms for such toughening. The work-to-fracture registered for PLCNF-10 surpasses that of other natural and synthetic composites, attesting to the excellent performance offered by the nanostructured PLCNF/PVA composites. For instance, values reported for collagen, bone, and natural rubber

are 2.8, 3.0, and 10.0 MJ.m^{-3}, respectively. Composites based on HEC as a matrix and CNF or bacterial cellulose as reinforcement registered a work to fracture of 27.1 and 11.0 MJ.m^{-3}, respectively [44,45]. Nonetheless, it is important to note that at higher filler contents, polymer chain mobility may be restricted, potentially leading to a decrease in ductility and toughness. Overall, these findings demonstrate that PLCNFs serve as an effective reinforcement, improving simultaneously stiffness, strength, and ductility, which contrasts with the typical strength-ductility trade-off usually reported for CNC/CNF-reinforced PVA.

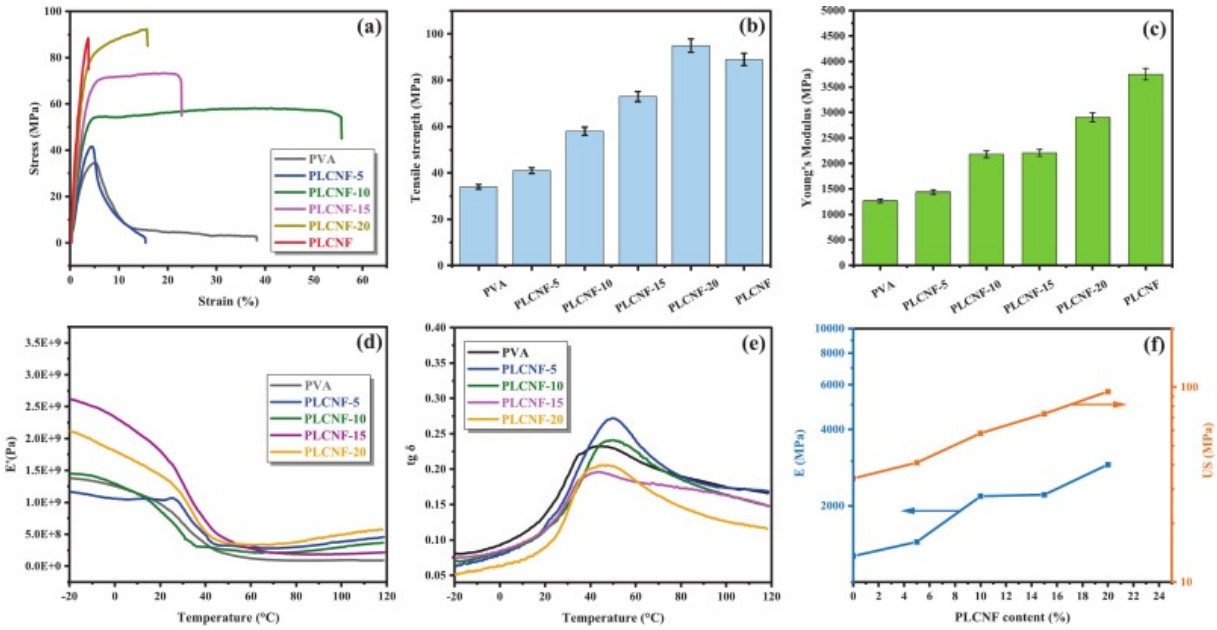

Fig. 10. (a) Stress vs. strain, (b) tensile strength, (c) Young's modulus, (d) storage modulus (E'), (e) tan δ, and (f) tensile modulus E and ultimate strength (US) of neat PVA, PLCNF, and PVA/PLCNF films with different concentrations (0, 5, 10, 15, and 20).

Furthermore, the presence of lignin within LCNFs has been demonstrated to impede their percolation and network-forming abilities, which are essential for improving mechanical performance. This disruptive effect arises from the lignin interfering with fibril-fibril interactions. However, prior studies suggest that when an entangled fibrillar network can still be established, the detrimental influence of lignin is mitigated, potentially leading to enhancements in ductility and toughness. Moreover, at moderate concentrations, lignin can exert a positive impact by acting as a natural binder or crosslinking agent, promoting stress transfer between individual fibrils and bolstering the mechanical integrity of the material [11].

As shown by DMA **(**Fig. 10, Fig. 10**),** the incorporation of PLCNFs significantly influenced the viscoelastic behavior of PVA films. At low PLCNF content (5 wt%), the storage modulus (E') increased by ~15 % compared to neat PVA in the glassy region. When PLCNF content exceeds 10 wt%, a significant reinforcement effect was observed, particularly across

the glass transition temperature (T_g). The PLCNF-15 nanocomposite exhibited the highest storage modulus (5.34 GPa), while PLCNF-20 still displayed a ~39 % increase in E' relative to neat PVA film in the glassy region. This trend indicates that an optimal dispersion and continuous nanofibril network formed at intermediate filler loading (15 wt%), whereas partial nanofibril aggregation at 20 wt% PLCNF may slightly reduce reinforcement efficiency in the glassy region.

Table 4. The effect of different (PVA/PLCNF) ratios on the mechanical properties of PVA composite films.

Sample	Tensile strength (MPa)	Young's modulus (MPa)	Strain at break (%)	Toughness ($MJ.m^{-3}$)	Yield stress (MPa)	T_g(°C)
PVA	34 ± 1.02	1266 ± 37.9	41.9 ± 5.4	3.5 ± 0.5	28.17 ± 0.44	43
PLCNF-5	41 ± 1.2	1440 ± 43.2	15.5 ± 1.3	2.6 ± 0.2	33 ± 3	50
PLCNF-10	58 ± 1.7	2180 ± 65.4	49.1 ± 9	30.5 ± 5.6	52.5 ± 1.5	49
PLCNF-15	73 ± 2.2	2209 ± 66.3	22.8 ± 0.4	15 ± 0.5	73.5 ± 3.5	44
PLCNF-20	95 ± 2.8	2905 ± 87.2	14.2 ± 3.4	12.3 ± 2.9	76 ± 4	47
PLCNF	89 ± 2.7	3750 ± 112.5	3.3 ± 0.7	2.1 ± 0.5	78.7 ± 6.4	–

In the rubbery region above T_g, all composites retained higher storage modulus values than neat PVA, demonstrating a better stability of the nanofibril network even at elevated temperatures. The tan δ curves **(**Fig. 10e**)** showed slightly lower peaks and broader transitions for PLCNF composites, indicating restricted chain mobility and improved elastic energy storage due to strong interfacial bonding between PVA and PLCNFs. The T_g shifted upward by ~1–7 °C upon PLCNF addition, further confirming strong polymer-filler interactions. These results demonstrate that PLCNFs not only stiffen the matrix in the glassy state but also improve the mechanical stability of the composite in the rubbery region. Overall, the reinforcing effect of PLCNF networks within the matrix is consistently reflected in both the dynamic and static mechanical data.

4. Conclusion

This work presents an eco-friendly approach for producing PLCNFs from lignocellulosic biomass and their incorporation into a PVA matrix to develop multifunctional biocomposites. The produced PLCNFs consisted of high aspect ratio 3–5 nm fibrils and 10–20 nm lignin spheres, with a charge content of 6100 $mmol.kg^{-1}$. Their incorporation imparted multifunctional properties to the PVA matrix. The lignin chromophore moieties enabled

significant UV shielding with less than 50 % UV absorption at 20 wt% PLCNF loading, accompanied by a moderate reduction in film transparency from ~90 % for neat PVA to 60–85 % PLCNF composites at 600 nm. Hydrophobicity increased with a contact angle of 53° for PLCNF-20 compared to 41° for neat PVA, while moisture uptake remained within a 10–15 % range at 75 % RH, a value that is comparable to neat PVA (11 %) and considerably lower than neat PLCNF film (27 %). FTIR confirmed strong PVA/PLCNF interactions via intermolecular hydrogen bonding, as evidenced by hydroxyl band shifts. Phosphate groups enhanced flame retardancy, yielding higher char residue and reduced PHRR, THR, and HRC compared to neat PVA. SEM observations revealed homogeneous PLCNF dispersion, forming a percolated fibrillar network, which resulted in nearly tripled tensile strength and Young's modulus at a 20 wt% PLCNF loading. Overall, the combined mechanical reinforcement, UV-shielding, and flame-retardant performance position these multifunctional nanocomposites as strong candidates for food packaging, protective coatings, and other applications requiring enhanced fire safety.

CRediT authorship contribution statement

Soumia Boukind: Writing – review & editing, Writing – original draft, Visualization, Methodology, Investigation, Formal analysis, Data curation, Conceptualization. **Wafa Cheikhrouhou:** Formal analysis. **Jean-Luc Putaux:** Writing – review & editing, Visualization, Formal analysis. **Sami Boufi:** Writing – review & editing, Visualization, Validation, Resources. **Houssine Sehaqui:** Writing – review & editing, Visualization, Validation, Supervision, Project administration.

Declaration of competing interest

The authors declare that they have no known competing financial interests or personal relationships that could have appeared to influence the work reported in this paper.

Acknowledgements

The authors gratefully acknowledge the Materials Science, Energy and Nanoengineering Department (MSN) at Mohammed VI Polytechnic University (UM6P) for financial support. They also thank Ms. Ihsane Kassem for assistance with SEM observations and the NanoBio-ICMG Platform (UAR 2607, Grenoble) for granting access to the Electron Microscopy Facility.

References

1. Trigui K, Magnin A, Putaux JL, Boufi S. Poly(vinyl alcohol)/oxidized cellulose nanofibril composite films with high nanofiller content for enhanced packaging applications. J Ind Eng Chem 2025;148:602–613. https://doi.org/10.1016/j. jiec.2025.01.016.
2. Wu Y, Tang Q, Yang F, Xu L, Wang X, Zhang J. Mechanical and thermal properties of rice straw cellulose nanofibrils-enhanced polyvinyl alcohol films using freezing- and-thawing cycle method. Cellulose 2019;26:3193–3204. https://doi.org/10.1007/ s10570-019-02310-6.
3. Wang M, Miao X, Li H, Chen C. Effect of length of cellulose nanofibers on mechanical reinforcement of polyvinyl alcohol. Polymers 2022;14:1–16. https://doi.org/10.3390/polym14010128.
4. Mahardika M, Masruchin N, Amelia D, Ilyas RA, Septevani AA, Syafri E, et al. Nanocellulose reinforced polyvinyl alcohol-based bio-nanocomposite films: improved mechanical, UV-light barrier, and thermal properties. RSC Adv 2024;14: 23232–9. https://doi.org/10.1039/d4ra04205k.
5. Serra-Parareda F, Tarrès Q, Sanchez-Salvador JL, Campano C, Pèlach MA, Mutjé P, et al. Tuning morphology and structure of non-woody nanocellulose: Ranging between nanofibers and nanocrystals. Ind Crop Prod 2021;171:113877. https://doi.org/ 10.1016/j.indcrop.2021.113877.
6. Trache D, Tarchoun AF, Derradji M, Hamidon TS. Nanocellulose: from fundamentals to advanced applications. Front Chem 2020;8:392. https://doi.org/ 10.3389/fchem.2020.00392.
7. Kargarzadeh H, Mariano M, Gopakumar D, Ahmad I, Thomas S, Dufresne A, et al. Advances in cellulose nanomaterials. Cellul 2018;25:2151–2189. https://doi.org/ 10.1007/s10570-018-1723-5.
8. Yu S, Sun J, Shi Y, Wang Q, Wu J, Liu J. Nanocellulose from various biomass wastes: its preparation and potential usages towards the high value-added products. Environ Sci Ecotechnol 2021;5:100077. https://doi.org/10.1016/j. ese.2020.100077.
9. Tyagi P, Gutierrez JN, Nathani V, Lucia LA, Rojas OJ, Hubbe MA, et al. Hydrothermal and mechanically generated hemp hurd nanofibers for sustainable barrier coatings/films. Ind Crop Prod 2021;168:113582. https://doi.org/10.1016/j. indcrop.2021.113582.
10. Zhang Y, Haque ANMA, Naebe M. Lignin–cellulose nanocrystals from hemp hurd as light-coloured ultraviolet (Uv) functional filler for enhanced performance of polyvinyl alcohol nanocomposite films. Nanomaterials 2021;11:3425. https://doi.org/ 10.3390/nano11123425.
11. Najahi A, Tarr´es Q, Mutj´e P, Delgado-Aguilar M, Putaux JL, Boufi S. lignin-containing cellulose nanofibrils from TEMPO-mediated oxidation of date palm waste: preparation, characterization, and reinforcing potential. Nanomaterials 2023;13:126. https://doi.org/10.3390/nano13010126.
12. Ye J, Xu Q, Gao Y, Liang Y, Wu Q, Wu G, et al. Flexible, transparent, and fire-proof cellulose nanofibril films with outstanding flame retardancy. Ind Crop Prod 2024; 211:118210. https://doi.org/10.1016/j.indcrop.2024.118210.
13. Xu ZC, Yang YQ, Pang XW, Jiang B, Mao PF, Gong LX, et al. Rapid gelation of mechanical robust, conductive, and self-healing lignocellulosic nanofibrils hydrogel toward flexible sensor over a broad temperature spectrum. Chem Eng J 2025;503:158243. https://doi.org/10.1016/j.cej.2024.158243.
14. Xu ZC, Yang YQ, Pang XW, Xu YT, Gong LX, Tang LC, et al. Mechanical tough, non- swelling, self-adhesive and highly conductive amphibious hydrogels for motion sensing in complex conditions. J Mater Sci Technol 2025;237:10–19. https://doi. org/10.1016/j.jmst.2025.02.052.
15. Wang X, Jia Y, Liu Z, Miao J. Influence of the lignin content on the properties of poly(lactic acid)/lignin-containing cellulose nanofibrils composite films. Polymers 2018;10:1013. https://doi.org/10.3390/polym10091013.
16. Bian H, Wei L, Lin C, Ma Q, Dai H, Zhu JY. Lignin-containing cellulose nanofibril- reinforced polyvinyl alcohol hydrogels. ACS Sustain Chem Eng 2018;6:4821–4828. https://doi.org/10.1021/acssuschemeng.7b04172.
17. Peng Y, Nair SS, Chen H, Yan N, Cao J. Effects of lignin content on mechanical and thermal properties of polypropylene composites reinforced with micro particles of spray dried cellulose nanofibrils. ACS Sustain Chem Eng 2018;6:11078–11086. https://doi.org/10.1021/acssuschemeng.8b02544.
18. Wu Z, Wu J, Peng T, Li Y, Lin D, Xing B, et al. Preparation and application of starch/polyvinyl alcohol/citric acid ternary blend antimicrobial functional food packaging films. Polymers 2017;9:102. https://doi.org/10.3390/ polym9030102.

19. Zhang X, Tanguy NR, Chen H, Zhao Y, Gnanasekar P, Le Lagadec R, et al. Lignocellulosic nanofibrils as multifunctional component for high-performance packaging applications. Mater Today Commun 2022;31:103630. https://doi.org/ 10.1016/j.mtcomm.2022.103630.
20. Fu H, Li Y, Wang B, Li J, Zeng J, Li J, et al. Structural change and redispersion characteristic of dried lignin-containing cellulose nanofibril and its reinforcement in PVA nanocomposite film. Cellullose 2021;28:7749–7764. https://doi.org/10.1007/ s10570-021-04041-z.
21. Mutuyimana A, Boukind S, Ablouh EH, Cherkaoui O, Khalili H, Jaworski A, et al. Straightforward association of phosphate with giant reed fibers for rapid and efficient water decontamination. Carbohydr Polym 2025;357. https://doi.org/ 10.1016/j.carbpol.2025.123470.
22. Iwamoto S, Kai W, Isogai A, Iwata T. Elastic modulus of single cellulose microfibrils from tunicate measured by atomic force microscopy. Biomacromolecules 2009;10: 2571–2576. https://doi.org/10.1021/bm900520n.
23. Saito T, Kuramae R, Wohlert J, Berglund LA, Isogai A. An ultrastrong nanofibrillar biomaterial: the strength of single cellulose nanofibrils revealed via sonication- induced fragmentation. Biomacromolecules 2013;14:248–253. https://doi.org/ 10.1021/bm301674e.
24. Saito T, Nishiyama Y, Putaux JL, Vignon M, Isogai A. Homogeneous suspensions of individualized microfibrils from TEMPO-catalyzed oxidation of native cellulose. Biomacromolecules 2006;7:1687–1691. https://doi.org/10.1021/bm060154s.
25. Nechyporchuk O, Belgacem MN, Bras J. Production of cellulose nanofibrils: a review of recent advances. Ind Crop Prod 2016;93:2–25. https://doi.org/10.1016/ j.indcrop.2016.02.016.
26. Kim HJ, Roy S, Rhim JW. Effects of various types of cellulose nanofibers on the physical properties of the CNF-based films. J Environ Chem Eng 2021;9:106043. https://doi.org/10.1016/j.jece.2021.106043.
27. Rol F, Belgacem N, Meyer V, Petit-Conil M, Bras J. Production of fire-retardant phosphorylated cellulose fibrils by twin-screw extrusion with low energy consumption. Cellulose 2019;26:5635–5651. https://doi.org/10.1007/s10570-019- 02447-4.
28. Liu C, Li MC, Chen W, Huang R, Hong S, Wu Q, et al. Production of lignin- containing cellulose nanofibers using deep eutectic solvents for UV-absorbing polymer reinforcement. Carbohydr Polym 2020;246:116548. https://doi.org/ 10.1016/j.carbpol.2020.116548.
29. Xiong F, Han Y, Wang S, Li G, Qin T, Chen Y, et al. Preparation and formation mechanism of renewable lignin hollow nanospheres with a single hole by self- assembly. ACS Sustain Chem Eng 2017;5:2273–2281. https://doi.org/10.1021/ acssuschemeng.6b02585.
30. Li Y, Chen Y, Wu Q, Huang J, Zhao Y, Li Q, Improved hydrophobic, UV barrier and antibacterial properties of multifunctional PVA nanocomposite films reinforced with modified lignin contained cellulose nanofibers Polymers 2022;14:1705. https://doi.org/10.3390/polym14091705.
31. Meeten GH, Optical properties of polymers, Elsevier London, New York, 1986, https://doi.org/10.1201/9781420057805.ch10.
32. Ait Benhamou A, Boukind S, Khalili H, Moubarik A, El Achaby M, Kassab Z, Sehaqui H. Strong and flame-resistant nanocellulose sheets derived from agrowastes via a papermaking-assisted process. ACS Appl Polym Mater 2024;6:2763-2776. https://doi.org/10.1021/acsapm.3c02941.
33. Yang H, Yu B, Xu X, Bourbigot S, Wang H, Song P. Lignin-derived bio-based flame retardants toward high-performance sustainable polymeric materials. Green Chem 2020;22:2129–2161. https://doi.org/10.1039/d0gc00449a.
34. Lyon RE, Walters RN. Pyrolysis combustion flow calorimetry. J Anal Appl Pyrol 2004;71:27–46. https://doi.org/10.1016/S0165-2370(03)00096-2.
35. Lyon RE, Walters RN, Stoliarov SI, Screening flame retardants for plastics using microscale combustion calorimetry, Polym Eng Sci 2007;47:1501–1510. https://doi.org/10.1002/pen.20871
36. Tong C, Zhang S, Zhong T, Fang Z, Liu H. Highly fibrillated and intrinsically flame- retardant nanofibrillated cellulose for transparent mineral filler-free fire-protective coatings. Chem Eng J 2021;419:129440. https://doi.org/10.1016/j. cej.2021.129440.
37. Zhang S, Li SN, Wu Q, Li Q, Huang J, Li W, et al. Phosphorus containing group and lignin toward intrinsically flame retardant cellulose nanofibril-based film with enhanced mechanical properties. Compos B Eng 2021;212:108699. https://doi.org/10.1016/j.compositesb.2021.108699.
38. Boukind S, Houssaine E, Mounir A, Achaby EL, Sehaqui H. Urea effect on cellulose phosphorylation and sustainable valorization of recycled washing filtrates. Waste Biomass Valoriz. Cellulose 2024;15:3239-3254. https://doi.org/10.1007/s12649-023-02376-1.

39. Velencoso MM, Battig A, Markwart JC, Schartel B, Wurm FR. Molecular firefighting—how modern phosphorus chemistry can help solve the flame retardancy task. Angew Chem Int Ed 2018;57:10450–10467. https://doi.org/10.1002/ anie.201711735.
40. Ghanadpour M, Carosio F, Larsson PT, Wågberg L. Phosphorylated cellulose nanofibrils: a renewable nanomaterial for the preparation of intrinsically flame- retardant materials. Biomacromolecules 2015;16:3399–3410. https://doi.org/ 10.1021/acs.biomac.5b01117.
41. Sehaqui H, EzekielMushi N, Morimune S, Salajkova M, Nishino T, Berglund LA. Cellulose nanofiber orientation in nanopaper and nanocomposites by cold drawing. ACS Appl Mater Interfaces 2012;4:1043–1049. https://doi.org/10.1021/am2016766.
42. Sehaqui H, Liu A, Zhou Q, Berglund LA. Fast preparation procedure for large, flat cellulose and cellulose/inorganic nanopaper structures. Biomacromolecules 2010; 11:2195–2198. https://doi.org/10.1021/bm100490s.
43. Henriksson M, Berglund LA, Isaksson P, Lindstro T. Cellulose Nanopaper Structures of High Toughness. Biomacromolecules 2008;9:1579–1585. https://doi.org/10.1021/bm800038n.
44. Vogel S. Comparative biomechanics: life's physical world. Princeton, NJ, Oxford: Princeton University Press; 2003.
45. Sehaqui H, Zhou Q, Berglund LA. Nanostructured biocomposites of high toughness—a wood cellulose nanofiber network in ductile hydroxyethylcellulose matrix. Soft Matter 2011;7:7342–7350.

Supplementary information

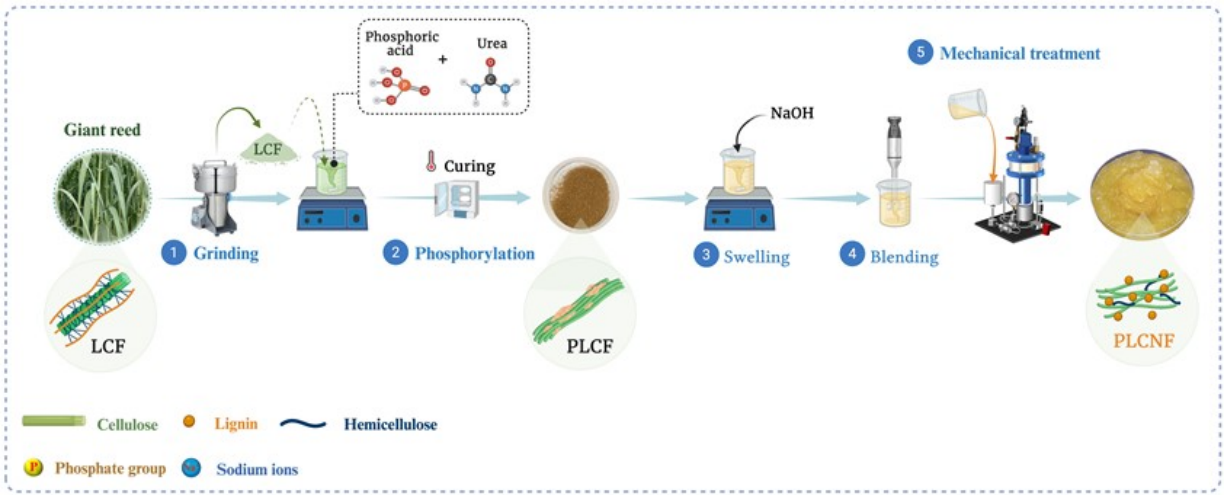

Fig. SI1. Flowchart of PLCNF production process.

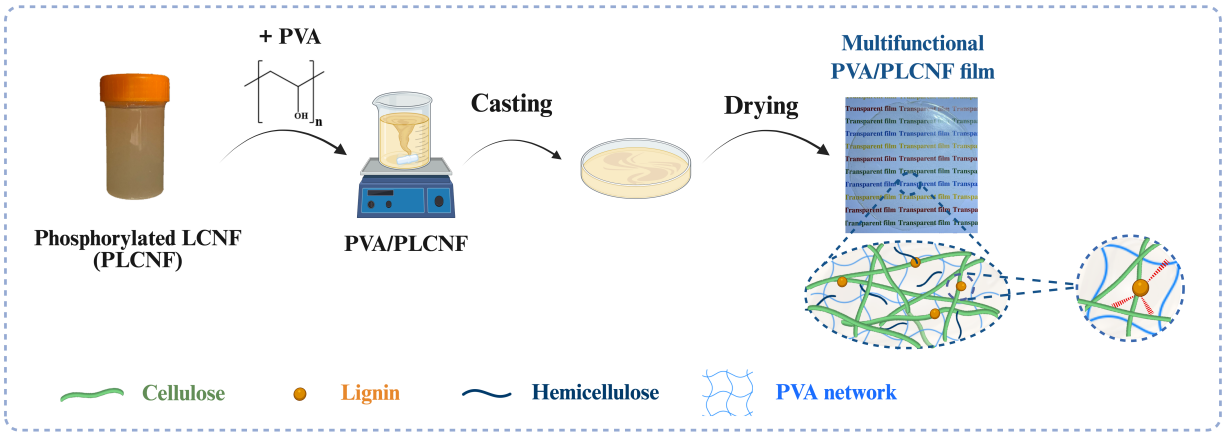

Fig. SI2. Schematic illustration of the production process for PVA/PLCNF composite films.

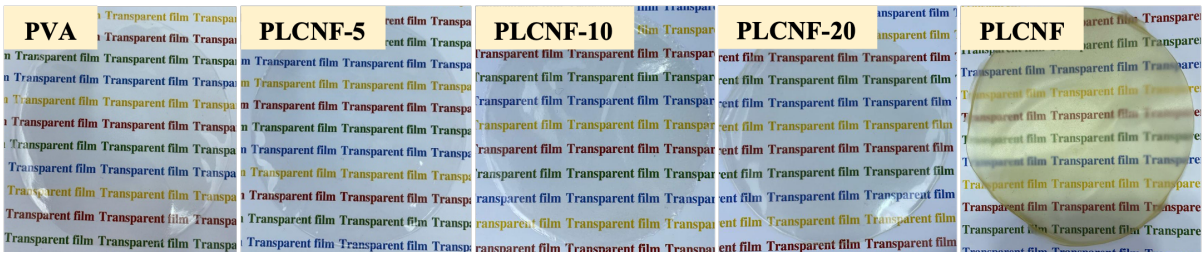

Fig SI3. Photographs of neat PVA, PLCNF, and PVA/PLCNF composite films with different PLCNF concentrations (0, 5, 10, 15, and 20 wt%).

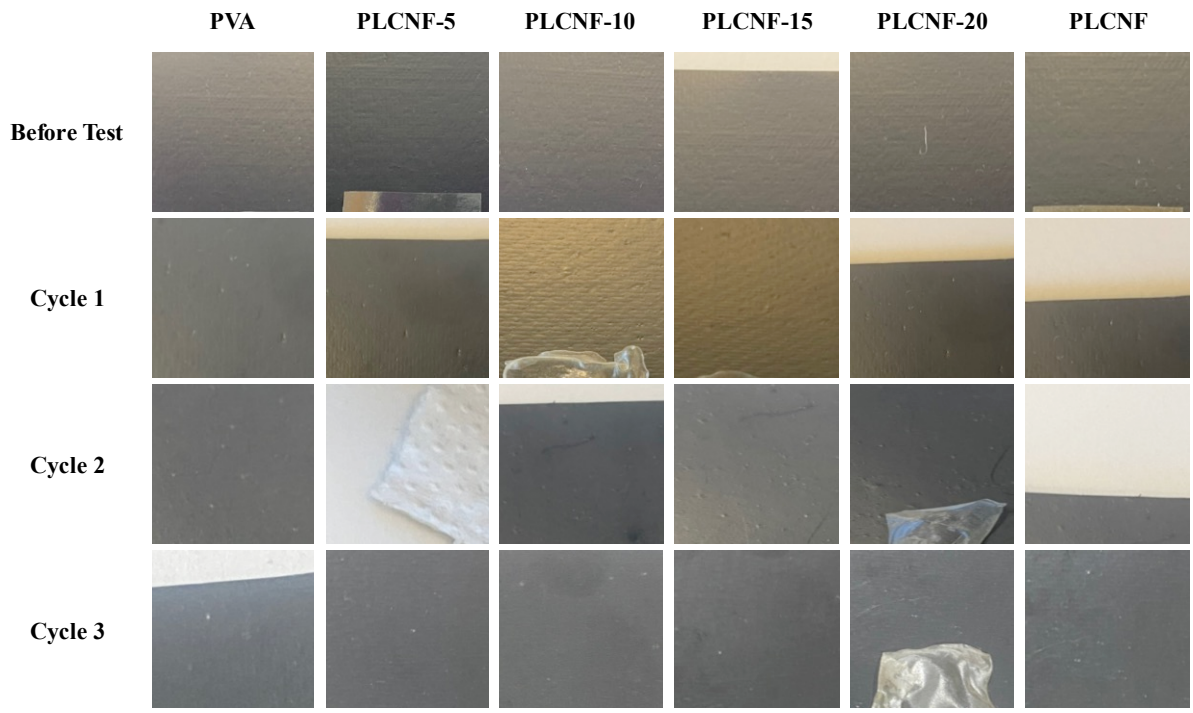

Fig. SI4. Photographs of neat and composite films before the washability test and after each immersion-drying cycle (cycles 1-3).